Design, Testing and Evaluation of Latching End Effector

B. Walker* and R. Vandersluis*

Abstract

The Latching End Effector (LEE) forms part of the Space Station Remote Manipulator System (SSRMS) for which Spar Aerospace Ltd, Space Systems Division is the prime contractor. The design, testing and performance evaluation of the Latching End Effector mechanisms is the subject of this paper focusing on a) ambient, thermal and vibration testing b) snare/rigidize performance testing and interaction during payload acquisition and c) latch/umbilical test results and performance.

Introduction

The Latching End Effector is a descendant of Shuttle Remote Manipulator System End Effector. The Space Station Arm required substantial increases in the life, load carrying capabilities, maintainability and reliability. The end effector design will a) provide compatibility with existing grapple fixture interfaces, b) provide a high-tolerance-to-misalignment payload interface and c) provide a stiff, backlash free interface with high load carrying capability.

Lee Design Overview

The complete Latching End Effector assembly (Figure 1) is an orbit replaceable unit. The Latching End Effector consists of the snare and rigidize subassembly inside the shell (Figure 2), and four latch/umbilical subassemblies outside the shell (Figure 3). The snare and rigidize mechanisms provides the capability to reduce large interface misalignments of free flying objects to the very accurate positioning required for latching. The latch mechanism was added to withstand large moment loads required by the larger payloads anticipated by Space Station use. An umbilical mechanism was built into the latch to provide an electrical connection for power and data across the end effector/payload interface.

Latching End Effector Mechanism Design & Development

The Latching End Effector design requirements for the space station were as follows:

a) compatibility with existing grapple fixtures as well as new Power Data Grapple Fixtures for the Space Station.
b) 30 second free flyer capture time (snare/rigidize and latch).
c) increased on-orbit life (without maintenance).
d) increased redundancy.
e) stiff, backlash free interface.
f) improved maintainability by on orbit replaceability of the entire end effector.

* Spar Aerospace Ltd, Space Systems Division, Brampton, Ontario, Canada

Snare/ Rigidize Mechanism

The snare mechanism motor module is mounted on the inner carriage. The motor drives through a three stage planetary gearbox to a segment gear mounted on a rotating ring (Figures 2 and 4) to which one end of each of the three snare cables are mounted. As the motor/gearbox drives the rotating ring with respect to the fixed ring the snare cables contact with the grapple shaft and wrap around the probe centering it (Figure 3). Once a successful snare has been completed, the snare brake is engaged and the rigidize mechanism can now be actuated.

The rigidize mechanism motor module, mounted on the rear outer shell and drives a two stage planetary gearbox (Figure 2). A ballscrew drives directly from the gearbox output mounted centrally in the rear outer shell. As the ballscrew rotates, the ballnut mounted on the inner carriage translates, moving the carriage along three sets of linear bushings mounted to the inside of the shell. A load cell located under the ballscrew measures the rigidize load.

After completion of the snare operation, the rigidize mechanism is commanded to retract the carriage. Initial carriage retraction (Figure 4) cause the snare cables to slide along the grapple shaft until the underside of the shaft end grapple cam contacted. The carriage continues to retract drawing the end effector and grapple fixture together until the three large grapple fixture cams align, first removing pitch and yaw misalignments (Figure 4), followed by the grapple cam/end effector pocket engagement to remove roll misalignments. Finally the two curvic couplings at the interface engage to remove backlash and provide precise alignment with the rigidize mechanism being preloaded to 4893 N (1100 lb).

Latch/Umbilical Mechanism

Each of the four latches consists of the parts shown in Figure 5. The tension bracket support and the ball nut pinion housing are stationary parts fixed to the shell. Four ball nut pinions driven by a ring gear on the outside of the shell (Figure 2), allows a single motor gearbox package to simultaneously drive the latches, maintaining the synchronization established at assembly.

The motor drives the ball screws moving the electrical connector carriers toward the grapple fixture in the sequence shown by Figures 6 through 9. The connector carrier rides on linear bearings (Figure 9) moving along tracks fixed to the shell.

Initially the sequencing rollers roll up the straight portion of the sequencing cams, holding the latch levers in their angled position. In this position, the latch deployment rollers are held captive by the levers causing the tension bracket to be pulled along with the connector carriers.

At the deployed position of the latch, the sequencing cam no longer restricts the movement of the levers. The disc spring stack's outer preload bushing has contacted the underside of the tension bracket support, preventing the tension bracket from moving any further unless the disc spring stack is compressed.

Continued movement causes the latch levers to spread, achieving the initial contact position (Figure 8). As the grapple fixture rollers continue to move up, the grapple fixture ramp, the pivot points on the latch lever (and thus the tension bracket) move up by about 3 mm. This movement compresses the belleville springs to result in a load between 16013 to 17125 N (3600 to 3850 lb) at each of the four latches. This 64054 N (14,400 lb) total load is a significant improvement over the 4894 N (1100 lb) rigidize load. This load applied at the curvic coupling teeth (Figure 1) at end effector/grapple fixture allows the capture and movement of large payloads without backlash or separation.

In the latched/connector mated position deployment rollers are on a "flat" portion of the latch lever (Figure 2). As the connector carrier moves between the connector mated position and the latched position (Figure 9) the compression of the disc spring stack remains constant. As the spring stack is not being compressed, the ball screw force required to move between the connector mated position and the latched position involves only overcoming bearing friction and the force to mate or demate the connector(about 222-445 N (50 to 100 lb) total)

The reverse delatch sequence is such that the disc spring stack is relaxing rather than being compressed. Since the disc springs are relaxing the retraction forces are substantially lower than the engagement forces.

Engineering Model Testing

In 1993, testing of the latching end effector and power data grapple fixture was carried out at ambient (room temperature) conditions and at hot and cold temperature extremes (representative of operating extremes in space). These tests were conducted after vibration testing (which simulated launch conditions), and after subjecting the end effector latched to the grapple fixture to structural loading (representative of the worst case loading conditions expected during operation and launch) and including representative simulation of capture envelope.

Test Rig Operation/Description

The Performance Test Rig design and geometry (Figure 10) articulates to enable the rig to simulate a pitch/yaw/roll misaligned end effector/grapple fixture interface. The test rig contains a data acquisition capability for real time monitoring of all mechanism parameters, the applied and reacted loads, and test rig position (in 6 Degrees of Freedom) during various misalignment simulations. The test rig also provides representative worst external joint load during capture.

Data Acquisition

Raw data was recorded at 50 millisecond intervals, in ASCII format. The forces in the mechanism; the motor current; the open or closed status of microswitches, a count of motor revolutions (from the motor resolver) multiplied by appropriate gear ratios so as to represent travel of the mechanism were measured as a function of time. The software also calculated the speed of the mechanism over the 50 millisecond intervals.

Data Reduction

Initial tests were run at a slow speed requiring up to 80 seconds for a latch/delatch resulting in 28,800 numbers for a single test. A dozen tests run at this speed resulted in 345,600 numbers. This amount of data becomes overwhelming if not summarized.

For the latch/umbilical results, computer spreadsheet macro analysis was used to determine the average value, and maximum and minimum value for each of the recorded parameters over each one tenth inch travel increment for each individual test. These values were then attributed to the average travel over the increment. As long as the extremes (max and min) and the average values compared favorably to the expected theoretical results the individual test run was considered to be successful.

The range of values of the seven latch ambient tests at slow speed was small and showed no significant variations. These test runs were considered as a consistent stable homogeneous group of results. Because of this, further summarization of all the ambient test at the slow speed was done. The overall average, overall maximum and overall minimum values of the variables in these seven test runs (Figure 15) became the criteria representative of "normal and expected" results; to be used to judge further test results against.

In the case of snare/rigidize mechanisms, performance is more directly influenced by the overall effect of misalignment loads during capture and hence the same detailed analysis is not required.

Normal and Expected Results

Having established a criteria for "normal and expected" results, it was found that changing the speed of latching from 40 seconds, to the normal operating speed requiring 6 seconds to latch had no significant effect. Similarly the comparison of slow speed for snare and rigidize to fast speed had no significant effect. Ambient test runs after the vibration tests, structural load tests also showed normal results.

Theoretical Results Compared to Test Results

Motor current is one of the more important test variables because from it the mechanism output force can be calculated. This is done by multiplying the current by the drive train gear ratio, by the drive train efficiencies assumed during analysis, by other appropriate constants which include the mechanism motor torque constant. The theoretical ball screw force was calculated based on the analysis of the equilibrium between (a) the ball screw force, (b) the sliding and rolling friction forces in the bearings, rollers and mechanism components, and (c) the forces in the belleville springs and structure as they were compressed.

For the snare mechanism, the determination of snare drive train torque must be translated from the gearbox to the cables mounted on the rotating ring as they are

wrapped around the probe thereby compress belleville springs mounted on the cable ends.

Snare/Rigidize Results

Snare

The snare mechanism ambient performance testing consisted of a series of runs from maximum grapple probe misalignment to fully aligned. The worst case capture scenario was with a radial offset was 4 inches, a pitch/yaw 15 degree misalignment and with a side load of 156 N (35 lb) (derived from the theoretical force to back drive the closest arm joint). A significant number of runs were performed under each misalignment case in order to verify performance of the mechanism. This data demonstrated mechanism repeatability under the various conditions.

Snare ambient performance is summarized in Figure 11. The highest current peaks occur at 0 and 75 degrees of rotation of the rotating ring. These high currrents at the start and finish of the snare represent the acceleration and deceleration of the high rotating inertia of the rotating ring. This motor load must then be accelerated (under closed loop control) to the maximum speed (300 $^{rad}/_{s}$), drive the snare cables to near end of travel (75 degrees) and decelerate the drive train within the maximum time of 3 seconds. The deceleration peak at 75 degrees is 0.5 amps lower than the acceleration peak, because of the cables tensioning and the 156 N (35 lb) external load, both act tend to slow the motor down, there by reducing the servo braking the motor must deliver.

The next load peak (Figure 11) is at 30 degrees and occurs at the maximum misalignment of the grapple fixture. Comparing this peak with subsequent peaks (as alignment is improved), shows the magnitude of the load is decreasing. This is a result of improved alignment geometry. Separating out dynamic inertia load effects from the constant 156 N (35 lb) radial load was accomplished by comparing the slow and fast snare runs. Fast snare operation runs were 5 times faster than the slow snare operation runs, resulting in the inertia load effect of 25 times greater. The much more benign slow speed runs (60 $^{rad}/_{s}$ motor speed) therefore allowed a relative comparison of the inertia effects versus the steady state 156 N (35 lb) radial load. The external loading from the rig (proportional to motor current[1]) correlated well to analytical predictions and control simulations. Overall mechanism performance with and without external loads was assessed by comparing snare (loaded and unloaded) as well as desnare performance to assess the mechanism performance in both directions.

Mechanism thermal and post vibration baseline tests were performed using the same test rig misalignment case (Figure 12). Thermal extreme runs were carried out and results were as anticipated. The cold case runs (-36° C) exhibited lower overall

---

[1] Separate motor module performance tests under similar ambient and thermal conditions enabled most of the uncertainties in assuming the current is proportional to the load (e.g., running friction, motor parameter variations) to be accounted for and hence removed from the absolute current for analysis purposes.

efficiency (i.e., higher torque to complete an operation). Hot (+71° C) snare operation resulted in the lowest torque. The ambient run was consistent with previous runs.

Rigidize
Rigidize testing simulated both worst case payload misalignment (15 degrees pitch/yaw and 10 degrees roll offset and an axial offset) and the best case with only the axial misalignment. The test rig imposed a 448 N (100 lb) axial load to simulate an average arm back driving while rigidizing. Friction in the rigidize mechanism was higher than expected, therefore current could not be relied on as an indicator of applied load. This was overcome by using the rigidize load cell (Figure 3) which provided axial load measurement as well as the strain gauged grapple shaft.

As with the snare ambient performance, dynamic loading was found to have a significant effect particularly under high speed, and at maximum misalignment conditions. Again it was found that dynamic loads could be accounted by comparison of the fast and slow runs. This in turn leads to a better understand and analysis the effects of the alignment load effects. Rigidization of loaded grapple shafts was compared to unloaded rigidizations in the absence of a grapple shaft. Loaded rigidize data was compared to unloaded derigidize operation provided bidirectional test results.

Rigidize mechanism thermal and post vibration baseline tests were performed using only the axial/longitudinal misalignment (Figure 14). Unlike the other mechanisms, there was no appreciable difference between temperature extremes. In addition the current "ripple" seen consistently throughout the ambient runs is not present in the cold (-36° C) case.

The relationship between current and external force (including dynamic effects) were validated using the multiple degree of freedom test rig. The relative sliding and alignment forces were determined to be within acceptable limits. However testing still needs to be carried in thermal vacuum to complete interface validation.

Abnormal and Unexpected Results

Rigidize mechanism friction losses were higher than expected resulting in lower than expected efficiency. Disassembly showed a multiple source interference problem within the rigidize gearbox. The resultant design changes will be implemented on the Qualification Model LEE with the gearbox to be tested prior to integration to ensure the problem has been solved.

Latch/Umbilical Results

Normal Results
The average ball screw force during ambient testing has a peak value of 1081 N (243 lb) and the maximum 1214 N (273 lb)and minimum 1005 N (226 lb) peak for a +133/-75 N (+30/-17 lb) tolerance around the average value. These values correspond very well to the 1112 N (250 lb)maximum ball screw force per screw predicted in the

theoretical analysis. This fact leads to the conclusion that the analysis and the efficiencies assumed are correct.

Abnormal and Unexpected Results

During the thermal testing, test runs while the latch mechanism was at hot temperature extremes of 60 and 75°C showed no adverse results. However, each run at cold temperature extremes (at -25 and -36°C) showed that more motor current was required to achieve a the latched condition (Figure 16). For the cold cycles, the average ball screw force (based on the motor current) has a peak value of 1601 N (360 lb) and the maximum 1904 N (428 lb) and minimum 1468 N (330 lb) peak such that a tolerance of +302/-133 N (+68/-30 lb) applies around the average value. These values exceed the 1557 N (350 lb) worst case ball screw force per screw predicted in the analysis.

The theoretical worst case 1557 N (350 lb) ball screw force was expected to arise due to deterioration in the coefficients of friction late in the life of the mechanism. Maximum forces as large as the 1904 N (428 lb) were not anticipated this early in the life of the mechanism.

Causes of Abnormal Results

The bearings and ball screws used in the mechanism were standard catalogue items modified only in that they used dry lubricants suitable for space. Analysis of bearings and ball screws and their housing and shaft fits under cold temperature conditions showed that additional clearances over and above that offered by the standard catalogue items is required.

Bearings suitable for cold temperatures will be available for the next set of qualification tests. It is anticipated that a significant improvement in operation will result.

Problems Caused By Deceptive Spreadsheet Graphs

Figure 17 attempts to illustrate the average latch load as a function of travel at the various temperatures, using the graph generated by spreadsheet commands. The problem with this graph is in the region of 95 mm (3.74 in) of travel. At this travel there is an 3781 N (850 lb) variation in load due to the temperature variation. The graph also indicates that the 8896 N (2000 lb) load occurs over a 3.8 mm (0.15 in) travel range depending on the temperature. A rough calculation of the possible thermal expansion and contraction of a 304.8 mm (12 in) long latch made of aluminum and steel accounts for less than 0.127 mm (0.005 in) of this 3.8 mm (0.15 in)variation. These graphs seem to indicate an unexplained load variation not behaving according to our analysis.

After investigation of potential explanations, it was discovered that the problem was in the limitations of the spreadsheet graphs themselves. The spreadsheet can plot the five load curves (due to the various temperatures) on the same graph, if and only if the five curves have a common ordinate relating the five curves. Table 1 illustrates the problem considering only the temperature extremes and the ambient case. In order to

plot multiple curves on one grid the spreadsheet requires that column B, F, and J be plotted against the travel in column A.

In spite of the best efforts in generating this graph (by lining up the data to start when the current was first applied), by the time the travel in column A reaches 5.84 mm (0.23 in) the travel in column F is up to 6.35 mm (0.25 in) and column I is down to 4.57 mm (0.18 in) for a +0.51/-1.27 mm (+.02/-.05 in) travel plotting error. By the time column A gets to 5.00 inches of travel, this error has increased to +0.25/-5.84 mm (+.01/-0.23 in). Plotting errors like this are sufficient to explain our 12.7 mm (0.15 in) variation.

Table 2 (below Table 1) illustrates the result of a Macro written to overcome this problem. What the macro does is to take the travel data of column E (in Table 1) and place it below the data of column A. The force data from column F was then moved so that the appropriate latch force was opposite the appropriate travel which used to be in column E. Similarly column I was relocated into column A below the rest of the data and column K relocated appropriately. The whole spreadsheet is then sorted so that column A is in ascending order. The columns B, F, and J remain associated with the appropriate travel of column A during this sort. This results in column A having a number in every space and columns B, F, and J having some values and some blank spaces between them.

Looking at table 2 illustrates this. Each of the values enclosed by a rectangle represents the number that exist after the above sorting process for which a corresponding set of values can be found in Table 1. The values that are not enclosed by a rectangle are blank at this point. The macro then goes down rows B, F, and J and linearly interpolates loads values between the values in the rectangles to correspond to the travel values in column A. The result is as illustrated in Table 2. The plot of this data gives a true picture of the relationships between the load data at various temperatures as shown in Figure 18. The reason for the now true representation is that each and every load ordinate has a corresponding travel abscissa, and each and every abscissa has a corresponding ordinate in each column.

It was felt that additional analysis was required to demonstrate that the original spreadsheet graphs were deceptive. The load/travel curves (Figure 17) all consist of 4 approximately straight lines 0 to 76.2 mm(0 to 3 in) travel, 88.9-94 mm (3.5 to 3.7 in), 101.6-114.3 mm (4 to 4.5 in), and 121.9-129.5 mm (4.8 to 5.1 in). These 4 lines are joined to each other by relatively sudden curves. Somewhere in these curved regions are the points at which the four straight lines would intersect if they were truly straight lines. This point at which the lines intersect will be referred to as the "point of inflection".

For each temperature, a spreadsheet linear regression analysis of the "straight lines" was carried out. Using the equations of the linear regression lines allowed the determination of the points of inflection. The various points of inflection occurred essentially at the same place within a +/- tolerance of about 0.762 mm (0.030 in). The 578 N (130 lb) load variation around the average 16605 N (3733 lb) load at 127 mm (5 in) of travel of Figure 18 is about a 3.5 % variation. This variation due to different temperatures is half of the 7 % predicted load variation. This prediction was based on

the fact that at high temperatures the modulus of elasticity of the disc springs is expected to change and the spring rate is expected to soften. This variation in itself is sufficient to explain the ±0.762 mm (+/- 0.030 in) tolerance on the point of inflection and convince skeptics that the problems of Figure 17 are due to the limitations of the spreadsheet graphing capability.

Discussion and Conclusions

These tests demonstrated a sophisticated (real time data acquisition) test rig simulation of the snare/rigidize process. The performance was verified in both thermal and ambient performance environments.

The tests show that having a multitude lot of test data is easier to handle as long as computers are available to analyze and summarize the data into a comprehensible summary.

However, the use of computers to reduce data to something that can be comprehended occasionally points to false conclusions (as with the deceptive graphs). Care must be taken to avoid the blind acceptance of computer generated data and the possible false conclusions that result.

In process testing (at subassembly level) would have highlighted the rigidize gearbox problems earlier in the design.

Cold temperature operation is the latch mechanism's most significant concern. Further qualification testing with bearings having suitable clearances calculated by our analysis should alleviate this concern.

A successful design and development program is dependent not only on theoretical analysis, but just as importantly on hardware testing that provides direct design validation and confidence in the analysis.

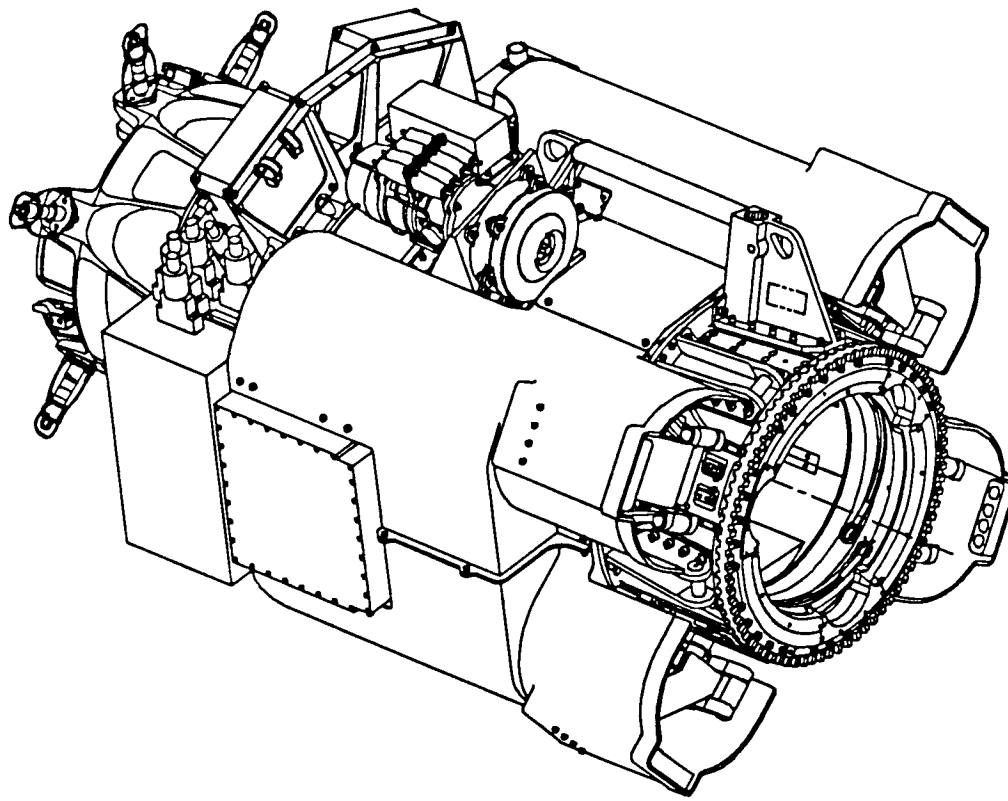

Figure 1 SSRMS Latching End Effector

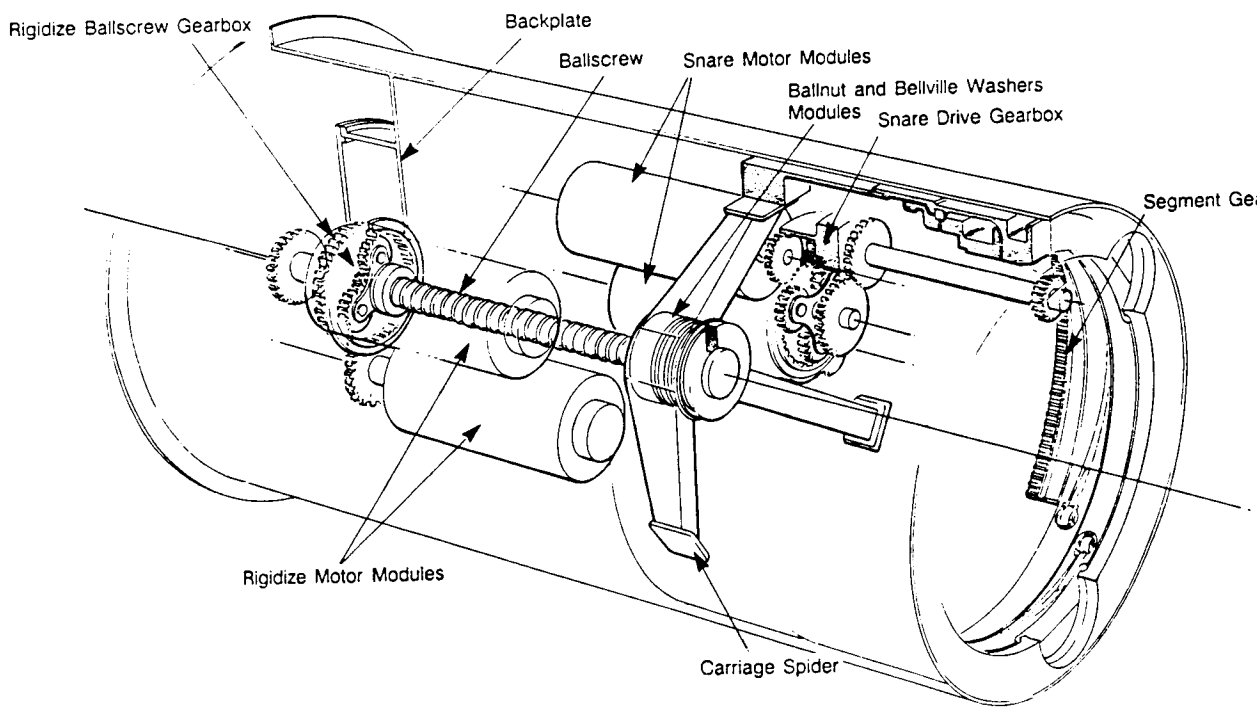

Figure 2 Snare/Rigidize Configuration

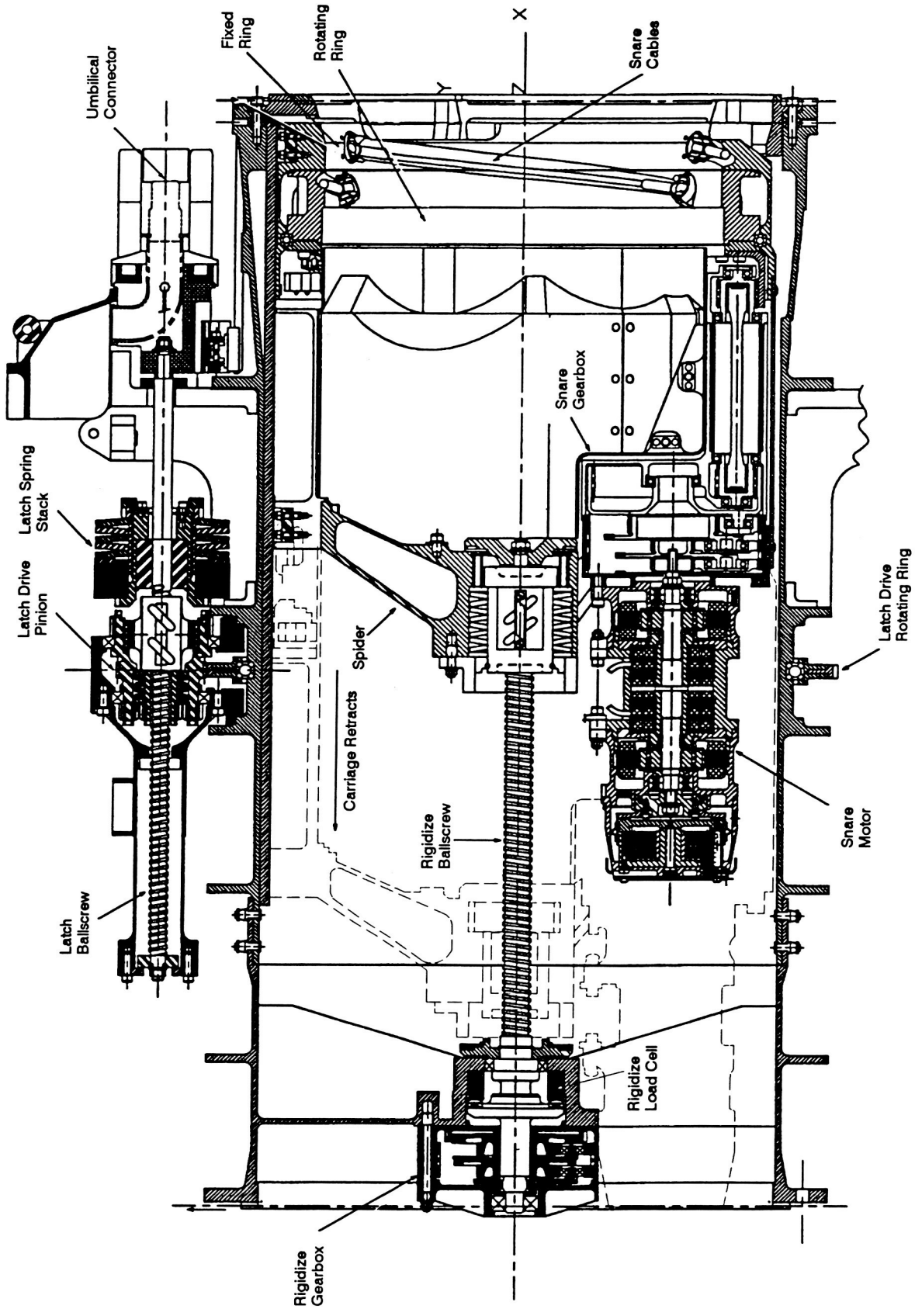

Figure 3 Snare/Rigidize Mechanisms

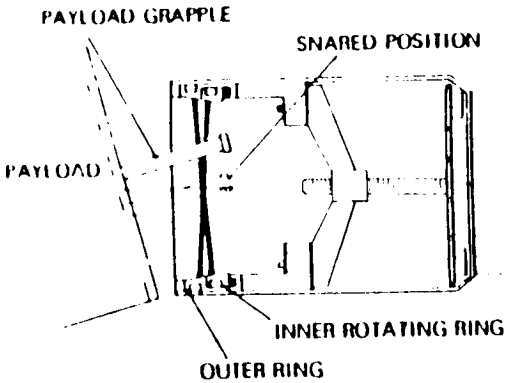

1
WITH RING IN FORWARD POSITION, WIRES STORED. PAYLOAD GRAPPLE ENTERS OPEN END OF EFFECTOR.

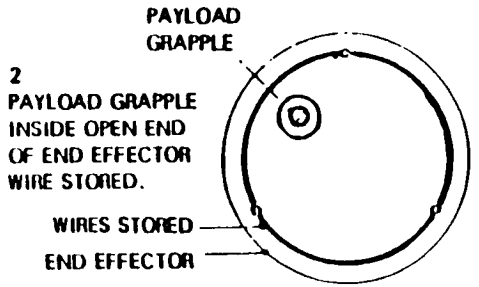

2
PAYLOAD GRAPPLE INSIDE OPEN END OF END EFFECTOR WIRE STORED.

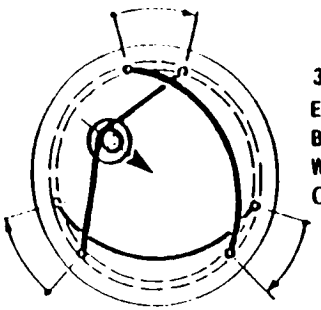

3
END EFFECTOR RING BEGINS TO ROTATE. WIRES BEGIN TO CLOSE ONTO PAYLOAD GRAPPLE.

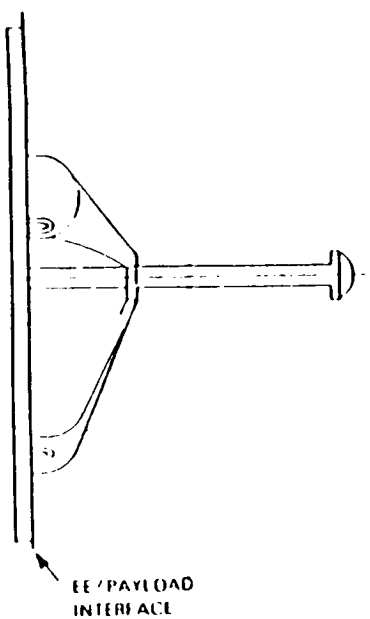

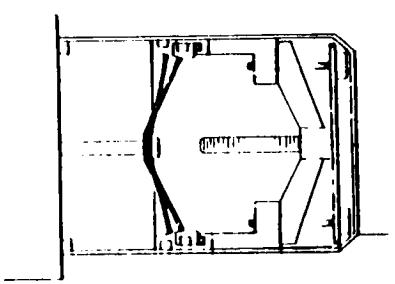

5
OPERATION OF BALL SCREW & NUT WITHDRAWS WIRES PULLING PAYLOAD INTO FULL CONTACT & KEYED ORIENTATION. FURTHER OPERATION TENSIONS WIRES RIGIDIZING THE CONTACT.

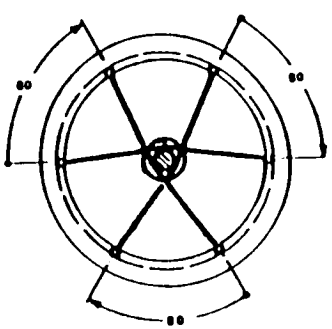

4
END EFFECTOR RING FULLY ROTATED. WIRES CLOSED ON PAYLOAD GRAPPLE, CENTERING IT & CAPTURING PAYLOAD.

Figure 4 LEE Capture/Rigidize Sequence

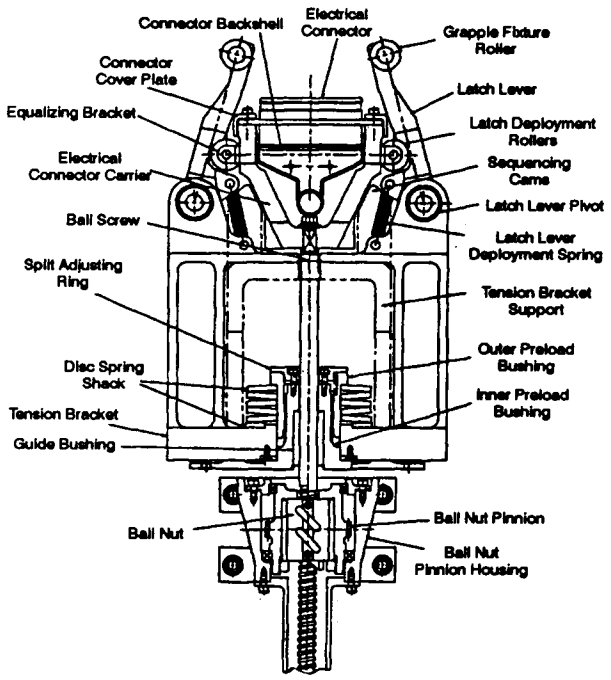

Figure 5 Latch Parts

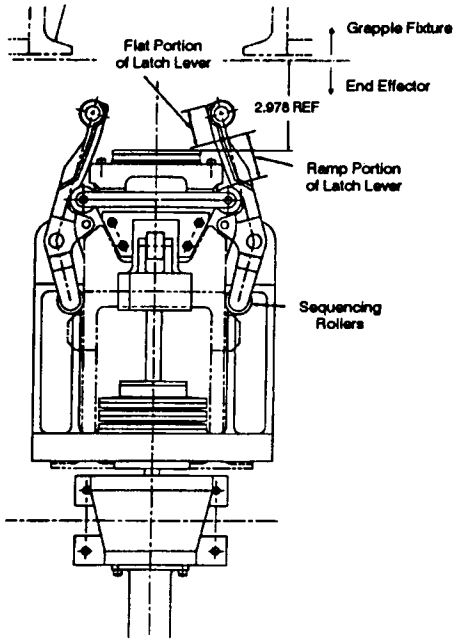

Figure 6 Fully Retracted Position

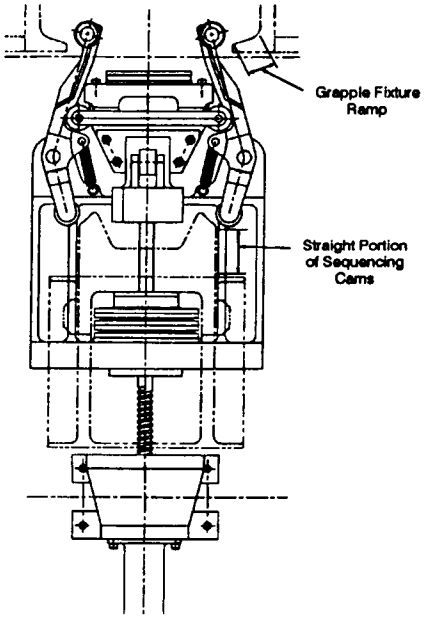

Figure 7 Deployed

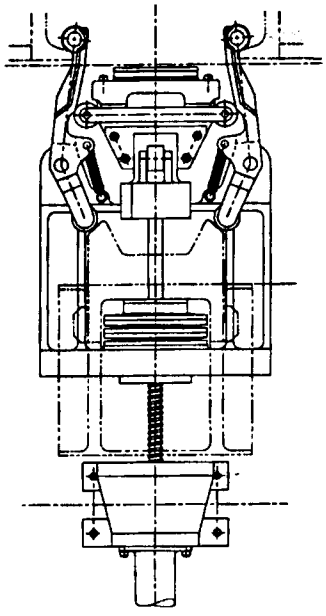

Figure 8 Initial Contact

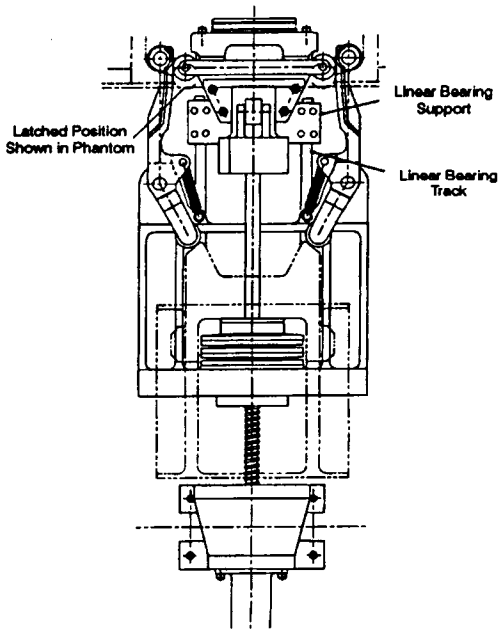

Figure 9 Latched and Mated Position

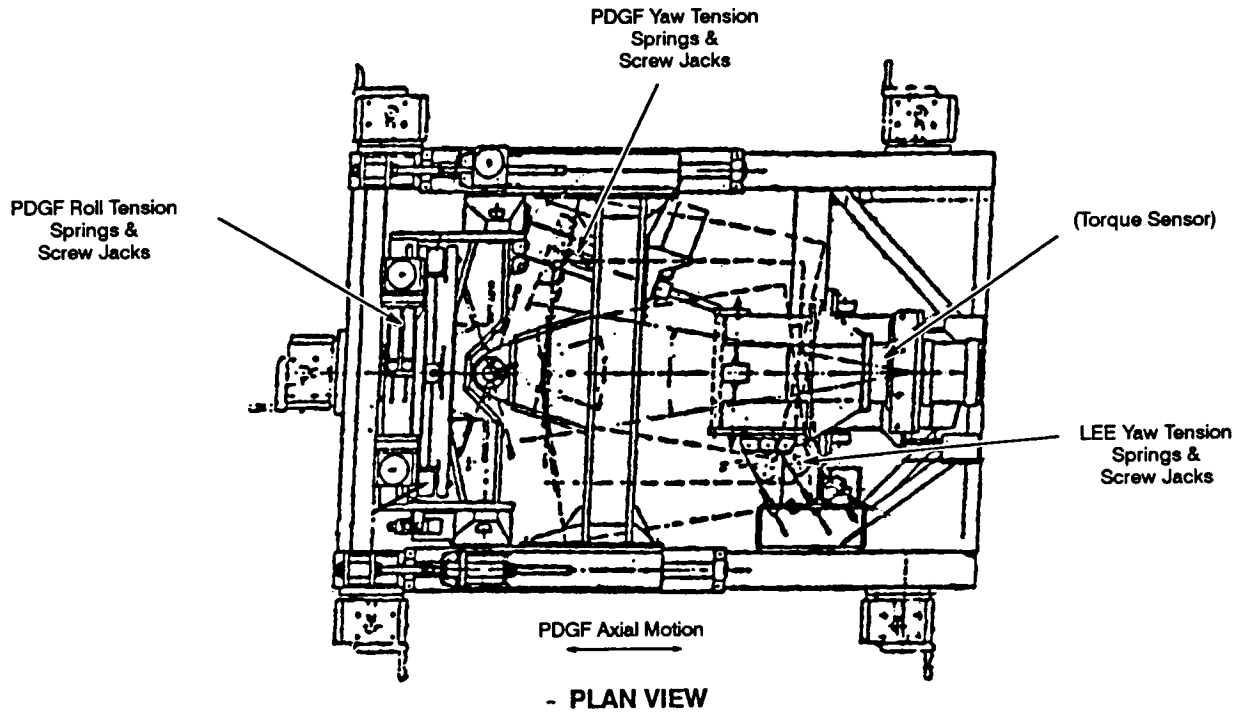

- PLAN VIEW

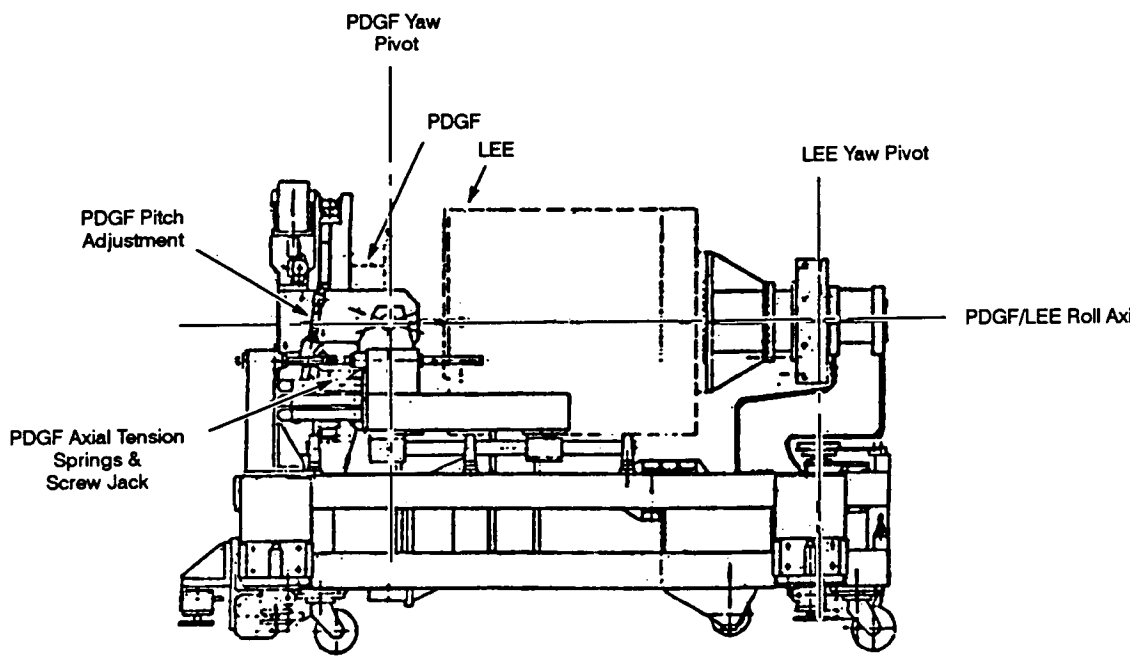

SIDE VIEW

Figure 10 LEEPTR General View

Snare Mechanism Ambient Performance

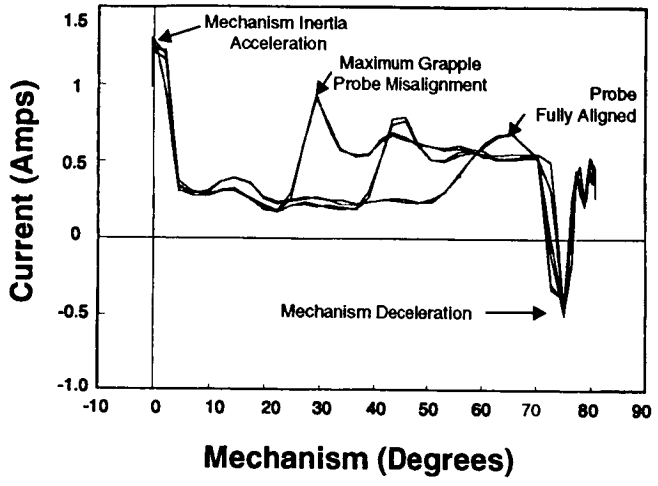

FIGURE 11

Snare Thermal Baseline Performance

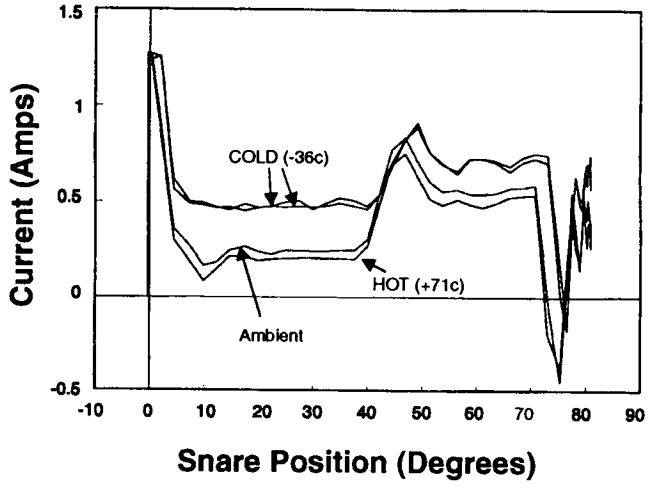

FIGURE 12

Rigidize Mechanism Ambient Performance

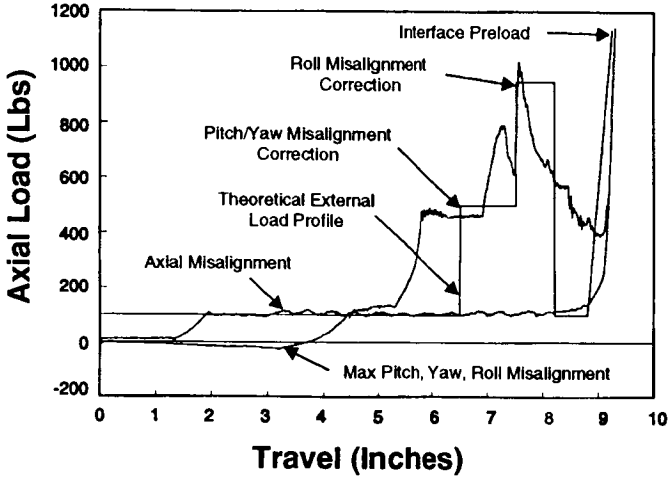

FIGURE 13

Rigidize Thermal Baseline Performance

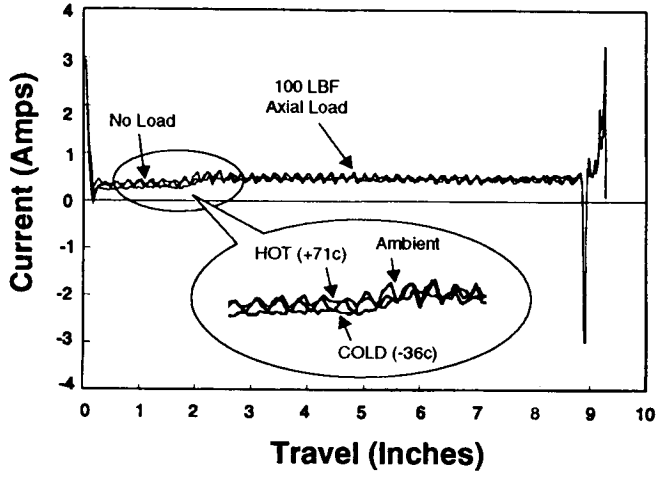

FIGURE 14

Ballscrew Force vs Travel
Seven Ambient Test Runs

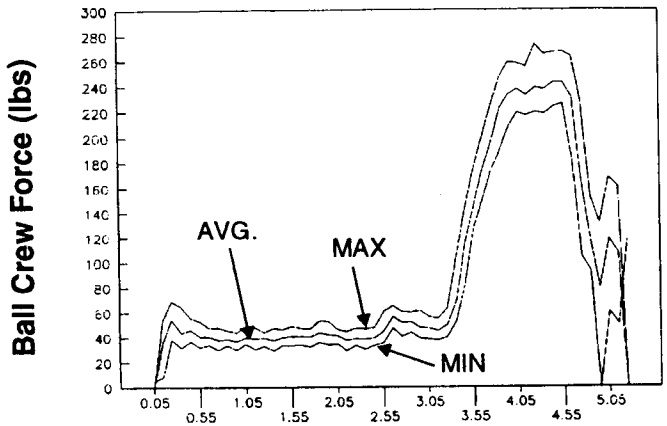

FIGURE 15

Current & Travel
Various Temperatures

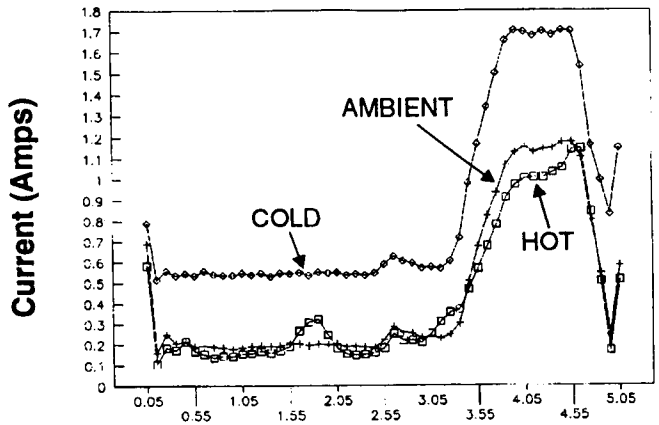

FIGURE 16

Latch Loads/Travel
Figure 8 - Temperatures as Noted

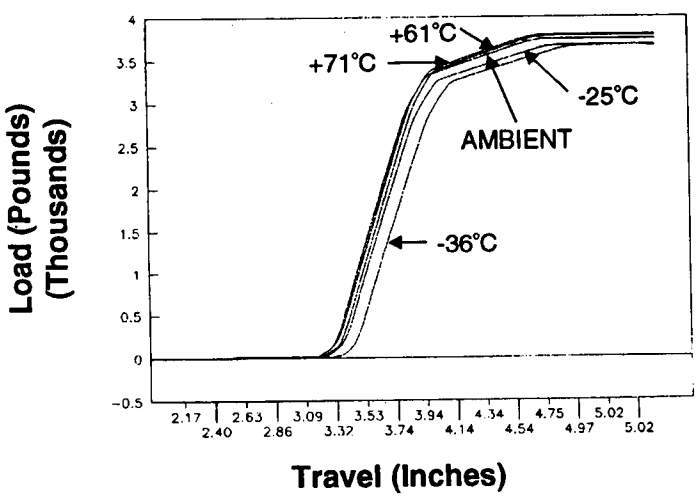

FIGURE 17

Load vs Travel After Corrections
Temperatures as Noted

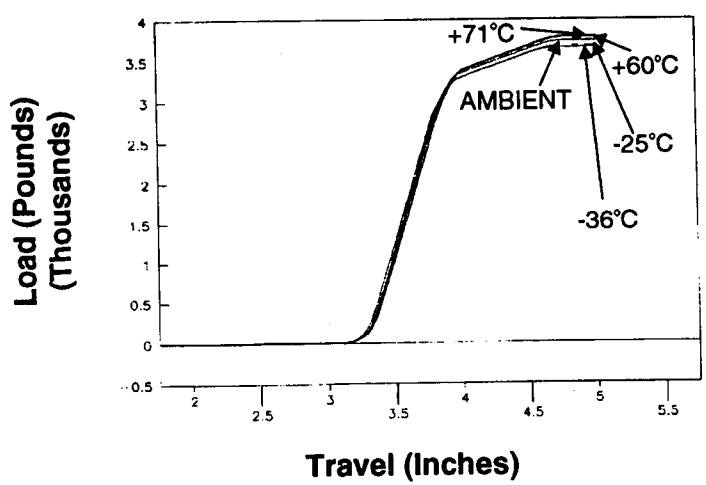

FIGURE 18